Journal of
Computational and Theoretical Nanoscience
Vol. 6, 1–9, 2009

Computations of Lossy Bloch Waves in Two-Dimensional Photonic Crystals

Christian Engström[1,*], Christian Hafner[2,*], and Kersten Schmidt[3]

[1] *Department of Mathematics, Karlsruhe University, Karlsruhe, Germany and Seminar for Applied Mathematics, ETH Zurich, Zurich, Switzerland*
[2] *Laboratory for Electromagnetic Fields and Microwave Electronics, ETH Zurich, Zurich, Switzerland*
[3] *Hausdorff Center for Mathematics and Institute for Numerical Simulation, University of Bonn, Germany*

In this article we compute lossy Bloch waves in two-dimensional photonic crystals with dispersion and material loss. For given frequencies these waves are determined from non-linear eigenvalue problems in the wave vector. We applied two numerical methods to a demanding test case, a photonic crystal with embedded quantum dots that exhibits very strong and anamolous dispersion. The first method is based on the formulation with periodic boundary conditions leading to a quadratic eigenvalue problem. We discretize this problem by the finite element method (FEM), first of quadratic order and, second, of higher orders using curved cells (p-FEM). Second, we use the multiple-multipole method (MMP) with artificial sources and compute extrema in the field response determining the eigenvalues. Both MMP and FEM provide robust solutions for the investigated dispersive and lossy photonic crystal, and can approximate the Bloch waves to a high accuracy. Moreover, the MMP method and p-FEM show low computational effort for very accurate solutions.

Keywords: Lossy Bloch Waves, Finite Element Method, Multiple-Multipole Method, p-FEM.

RESEARCH ARTICLE

1. INTRODUCTION

The pioneering work of Yablonovitch[1] and John[2] in 1987 caused a tremendous interest in artificial, nano-structured materials exhibiting band gaps in the area of visible light or at near infrared telecomm frequencies, namely because of the promise that photonic crystals will drastically reduce the packing density of integrated optics and because of rapid progress in fabrication technology.[3] The theoretical analysis of photonic crystals leads to eigenvalue problems of structures with periodic symmetry in one, two, or three directions. For reasons of simplicity, loss free photonic crystals are considered in the vast majority of the publications and most of the available software packages for computing band diagrams of photonic crystals omit material loss. Usually, either real-valued or purely imaginary frequency ω is considered as the corresponding eigenvalue, which is evaluated over the space spanned by the real-valued wave vector k. Propagating modes in a photonic crystal are then described by a real frequency, whereas evanescent modes exhibit an imaginary frequency. In practice, material losses are crucial for the value of photonic crystals as alternative to conventional integrated optics, photonic wires, and other concepts. In fact, losses cause important complications for the theoretical and numerical analysis. First of all, the frequency ω or the wave vector k must become complex. A complex frequency means that the modes decay in time. This description is usually used for the description of lossy resonators and for the extraction of the quality factor of resonators. A complex wave vector describes a wave attenuated along the direction of its propagation. This description is typical for waves propagating along waveguides. Since photonic crystals are used for creating resonators and waveguides, models with either a complex frequency or a complex wave vector are of interest. Several authors have investigated the former approach in the case of 2D metallic photonic crystals.[4–7]

In this paper, we focus on the evaluation of complex wave vectors for a given, real-valued frequency. We introduce two different finite element methods for the problem and compare the solutions with results published in the literature[9] and with the complex eigenvalue solver of the MMP code[10] contained in the MaX-1 (Ref. [11]) software package. Both FEM and MMP have the potential to be very accurate and are strong alternatives to the previously used methods.[6, 8, 9]

*Authors to whom correspondence should be addressed.

2. BLOCH WAVES AND EIGENVALUE PROBLEMS

The two-dimensional photonic crystal is a periodic medium described in terms of the underlying Bravais lattice.[12] The medium is characterized by a permittivity ε, with the periodicity of the lattice. We use a square lattice with lattice constant a and consider TM polarized waves in the crystal. In the TM case, where the electric field is in the z-direction, the electric field satisfies the equation

$$-\Delta E_z(x,y) = \frac{\omega^2}{c^2}\varepsilon(x,y,\omega)E_z(x,y) \tag{1}$$

where ω is the frequency and c is the speed of light in vacuum. A Bloch wave is a non-zero solution of the form

$$E_z(x,y) = e^{i(k_x x + k_y y)}u(x,y) \tag{2}$$

where u is a a-periodic function and $k = (k_x, k_y)$ is the (Floquet-Bloch) wave vector. Eigenfunctions of (1) can in a periodic medium be written in terms of Bloch waves.[13] We will consider Bloch waves that for a given real frequency decay in space. This class of waves is accessible from transmission experiments where the imaginary part of the wave vector is related to a reduced transmittance.

The translational symmetry of the permittivity implies that Bloch waves are determined from a problem over one cell in the lattice. For a fixed frequency ω, the Bloch waves can be determined from an eigenvalue problem in k. This eigenvalue problem is non-linear, which complicates the numerical computation. We will compare results from two different finite element methods (FEM) and the multiple-multipole method (MMP).

3. FINITE ELEMENTS

We reduce the spectral problem in the wave vector k to a problem in the complex amplitude λ of k in the direction v. Equation (1), with the ansatz (2), is multiplied by a periodic function w and integrated over one cell in the periodic lattice. Integration by parts gives

$$\lambda^2 a_2(u,w) + \lambda a_1(u,w) + a_0(u,w) = 0 \tag{3}$$

where

$$a_0(u,w) = \int \nabla u \cdot \nabla w^* - \frac{\omega^2}{c^2}\varepsilon u w^*\, dx\, dy,$$

$$a_1(u,w) = 2iv \cdot \int u \nabla w^*\, dx\, dy,$$

$$a_2(u,w) = \int u w^*\, dx\, dy$$

We search for periodic eigenfunctions u in an infinite dimensional space and complex eigenvalues λ such that (3) holds for all periodic functions w in the same space. We refer to Ref. [14] for a more detailed mathematical description of the problem. The eigenvalue problem for the Bloch solutions of TM polarized waves (3) is quadratic in λ, with the frequency ω as a parameter.

We discretize the eigenvalue problem (3) by a conforming Galerkin ansatz. The formulation used here was analyzed in Ref. [14] where the permittivity was assumed to be lossless. An approximate eigenfunction u is of the form

$$u = \sum_{j=1}^{N} c_j \phi_j$$

where ϕ_j are real basis functions defined piecewise on a FE mesh and the complex coefficients c_j are given by the solution of the quadratic matrix eigenvalue problem

$$\lambda_N^2 A_2 x + \lambda_N A_1 x + A_0 x = 0, \quad x = (c_1, \ldots, c_N)^T \tag{4}$$

where

$$(A_0)_{mn} = \int \nabla\phi_n \cdot \nabla\phi_m - \frac{\omega^2}{c^2}\varepsilon\phi_n\phi_m\, dx\, dy,$$

$$(A_1)_{mn} = 2iv \cdot \int \phi_n \nabla\phi_m\, dx\, dy,$$

$$(A_2)_{mn} = \int \phi_n\phi_m\, dx\, dy$$

The integrals above are over one cell in the crystal and v is the direction of the wave vector k. In this paper are the basis functions ϕ_n piecewise polynomials. We refer to Ref. [14] for a more detailed description of the discretization procedure.

The quadratic eigenvalue problem can be transformed to an equivalent generalized eigenvalue problem of double the dimension. This is important, because many robust numerical algorithms for computing eigenvalues are only available for linear eigenproblems. It is clear that there is a large number of different ways a quadratic eigenvalue problem can be linearized.[15] We use the linearization in Ref. [14], which has the advantage that the matrix B in the resulting linear problem $Ay = \lambda By$ is positive definite:

$$A = \begin{pmatrix} 0 & I \\ -A_0 & -A_1 \end{pmatrix} \qquad B = \begin{pmatrix} I & 0 \\ 0 & A_2 \end{pmatrix} \qquad y = \begin{pmatrix} x \\ \lambda x \end{pmatrix}$$

The computation of the eigenvalues can be done, for example, with the QZ-algorithm.[15] However, it turns out that this algorithm is not well suited for the computations, mainly for two reasons: First, the matrices are typically large and sparse. This is due to the fact, that they are generated by a finite element ansatz. The QZ-algorithm will destroy the sparsity in general and therefore lead to excessive storage requirements. Second, only a few eigenvalues need to be computed in order to determine the Bloch waves with lowest loss. For these reasons Krylov space methods, such as an implicitly restarted Arnoldi process (IRA) or an implicitly restarted Lanczos process (IRL), are preferable.[15] Using shift-and-invert strategies, these algorithms can be used to compute a small number of eigenvalues that are closest to a prescribed shift parameter.

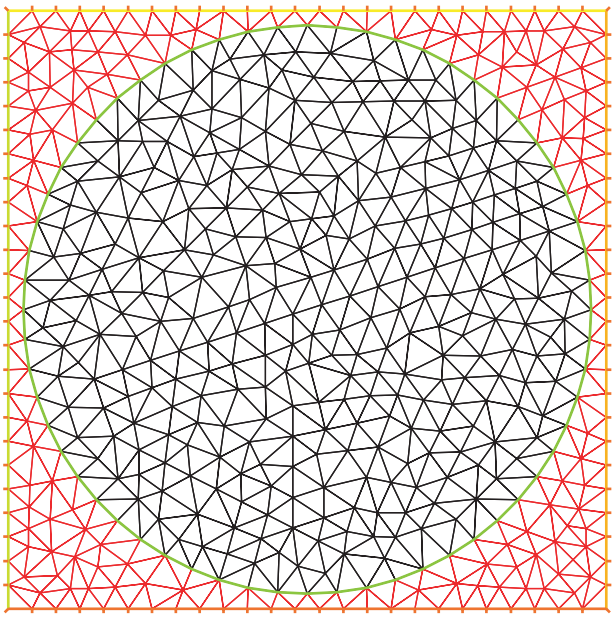

Fig. 1. The type of mesh used in the calculations with FreeFEM++.

In our numerical experiments we computed the M eigenvalues that are closest to zero with the IRA algorithm in the Matlab function eigs.[16]

For the discretization we use the numerical C++ libraries FreeFEM++ (www.freefem.org/ff++) and Concepts[17] (www.concepts.math.ethz.ch). The FreeFEM++ package uses quadratic basis functions on a triangular mesh. More accurate solutions results after refining the mesh where new nodes are inserted on curved material interfaces; see Figure 1. In contrast Concepts permits the use of higher order basis functions on curved

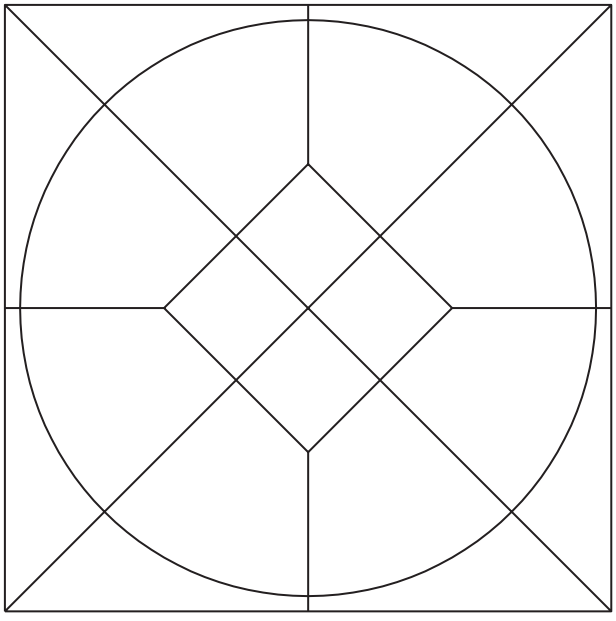

Fig. 2. Mesh with 20 curved quadrilateral cells used in the p-FEM computations with Concepts.

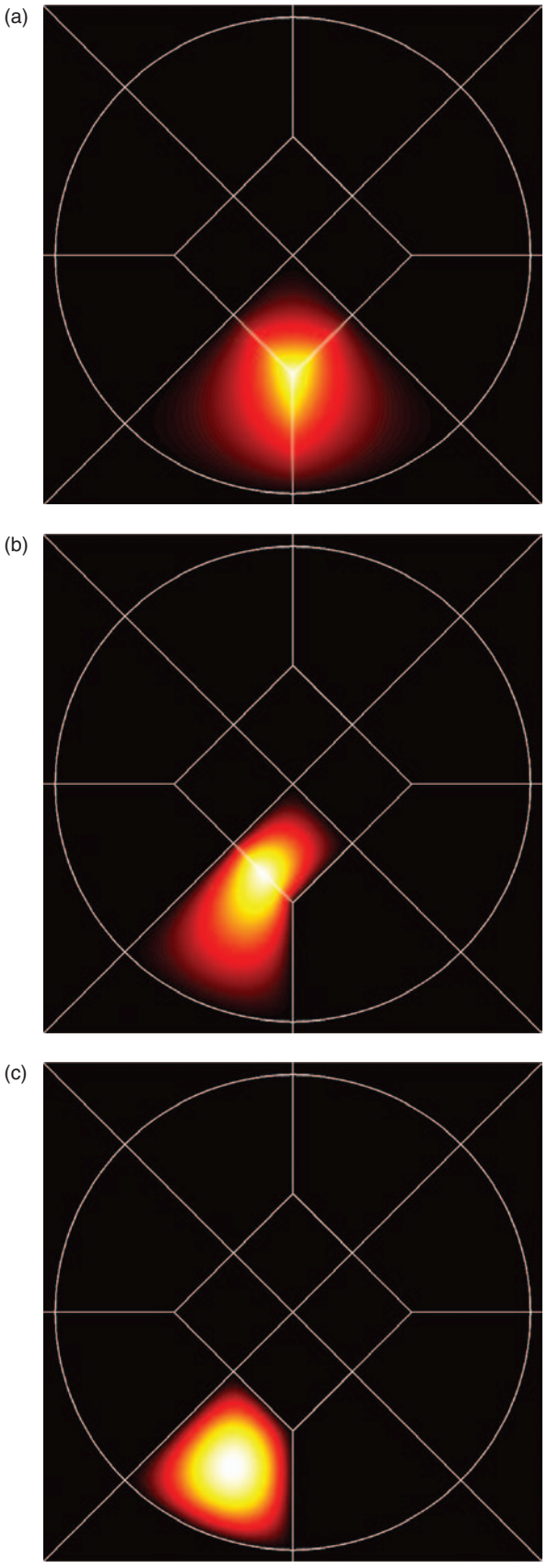

Fig. 3. Basis functions on the mesh with curved cells, (a) a vertex function, (b) an edge function and (c) inner or bubble function.

quadrilaterals whose edges can resolve exactly material interfaces. Hence, the p-version[18] of FEM can be used, i.e., the accuracy is increased by including basis functions of higher orders, but always using the same mesh; see Figure 2. The basis functions of each order are constructed as products of Jacobi polynomials in both directions of the reference square $[0, 1]$,[2] which are then mapped to a particular cell K in the mesh. Then, the matrix entries are computed by numerical quadrature on the reference square considering the deformation due to the cell maps.

For ensuring their continuity we classify the basis functions into vertex, edge and interior functions. The bilinear vertex functions are one on this vertex and vanish on opposite edges; see Figure 3(a). Edge functions are polynomials of degree $2, \ldots, p$ on this edge, fall linearly into the cell and vanish on all other edges; see Figure 3(b). An assembling procedure asserts for the continuity of all the vertex and edge functions over the cell edges. The continuity of the interior functions is trivial as they vanish on all edges; see Figure 3(c).

Using quadratic functions with FreeFEM++ leads to a moderate algebraic convergence, whereas with p-FEM on curved cells using Concepts one expects [18, 19] exponential convergence like $\exp(-\beta N^{1/2})$, where N is the number of degrees of freedom and β is a positive constant.

4. THE MULTIPLE-MULTIPOLE METHOD

MMP[10] is a semi-analytic boundary discretization method that approximates the electromagnetic field in each subdomain D_i separating different materials by a series expansion of the form

$$\text{Field}_i(\vec{r}) = \sum_{k=1}^{K_i} A_{ki} \cdot \text{Basis}(\vec{r}, \vec{r}_i) + \text{Error}(\vec{r}) \qquad (5)$$

where the basis fields are analytic solutions of Maxwell's equations. The amplitudes A_{ki} are optimized numerically in such a way that the continuity conditions for all field components on the boundaries of all subdomains are met. For obtaining reasonably short computation times, it is important to perform this optimization in such a way that a linear system of equations is obtained. In MMP, this is done by defining a weighted mismatching error along the boundaries and by minimizing its quadratic norm, which is essentially the same as in the method of weighted residuals. The error is only evaluated in a bunch of matching points but–unlike in standard point matching techniques–an overdetermined system of equations

$$RA = B + E \qquad (6)$$

is derived. Here, R is a rectangular system matrix, A the parameter vector containing the amplitudes A_{ki}, B a vector containing the excitation in the case of scattering problem, and E an error vector that is to be minimized. R essentially contains the basis fields and linear operators applied to the basis fields, sampled in the matching points.

In order to obtain solutions with minimal square norm of E one may multiply Eq. (6) with the adjoint matrix R^*. This leads to the normal equations with a hermitian matrix $S = R^*R$ and $R^*E = 0$. Unfortunately, this operation also squares the condition number of the system matrix. Since high condition numbers may lead to numerical errors, it is much better to solve (6) directly by means of QR decomposition.

In the case of eigenvalue problems of the form considered in this paper, the excitation vector B is missing. The eigenvalue λ then affects the basis fields and therefore all elements of the matrix R and one obtains the homogeneous equation

$$S(\lambda)A(\lambda) = 0 \qquad (7)$$

The eigenvalues λ are then obtained from the condition

$$\text{Det}(S(\lambda)) = 0 \qquad (8)$$

As mentioned before, it is much better to work with the overdetermined system of Eq. (6). For $B = 0$, this has the trivial solution $A = 0$ that is of no interest. For finding non-trivial solutions one can use several alternatives.

The simplest one is to re-establish an inhomogeneous system of equations of the form (6) by introducing a "fictitious" excitation that may be an arbitrary solution of Maxwell's equations, for example, a dipole source. A fictitious excitation mimics the excitation in real world experiments, typically the input port that feeds the resonating structure. In the real world experiment one also has at least one output port where the response of the system is measured. This may be done by introducing one or several "sensor points," where the field is evaluated. One then computes the response in all sensor points as a function $f(\lambda)$ of the eigenvalue and assumes that the peaks of the response represent the eigenvalues. This technique is often used in FDTD codes[20] and it is available in the MMP solver of the MaX-1 package.[11] However, it is not as trivial as one might believe. First of all, the search function $f(\lambda)$ depends on various parameters, the selection of the fictitious source, the sensor points, etc. When two eigenvalues are near to each other, they "melt together" and cannot be separated anymore. Furthermore, automatic eigenvalue detection leads to a demanding peak search and numerical inaccuracy may lead to the detection of multiple eigenvalues instead of a single one as in the double peak phenomenon.[21]

Another technique considers the error vector E in (6) as a function of the eigenvalue λ and searches for the minima of the square norm of E, which corresponds to the minimum residual technique. This approach suffers from frequently finding almost trivial solutions with small field values everywhere.[10] In order to avoid these almost trivial solutions, a more complicated iterative procedure was introduced in MMP: Here, the "last basis field" plays the role of the excitation and is moved to the right hand

side. Then (6) is solved using *QR* decomposition in such a way that square error norm is minimized. After this, the vector A is multiplied with a scaling factor in such a way that the sum of the amplitudes in all sensor points is equal to one. Implicitly, this means that one searches for minima of the function res(λ)/response(λ) or maxima of response(λ)/res(λ). This technique may be considered as an extension of the previous one. In many cases it allows one to separate several classes of modes by an appropriate selection of the "last basis field" and by an appropriate definition of the response.

Since one still may find pseudo-solutions in complicated situations, i.e., solutions with high relatively mismatching error along the boundary, MMP offers other eigenvalue search functions of the form error(λ)/response(λ), where error(λ) may be the absolute or relative, maximum or average mismatching error on the boundary or a combination of these four errors. This approach was successfully applied to very demanding cases.[7]

In the case of real eigenvalues, the MMP eigenvalue search is relatively simple. Assume that the eigenvalue λ depends on some parameter d. Fore example, d may be the frequency and λ may be the propagation constant of a waveguide. First one must restrict the parameter d to some finite interval $d_A < d < d_B$. When one searches for $\lambda_n(d_0)$ for a certain point d_0 in the given interval, one may first start a rough search by computing the eigenvalue search function

$$F(\lambda_n, d_0) = \text{error}^2(\lambda_n, d_0)/\text{response}^2(\lambda_n, d_0) \qquad (9)$$

in P points λ_n distributed uniformly over a search interval $\lambda_A < \lambda < \lambda_B$. Note that it is reasonable to introduce the squares in (9): If the response is measured in terms of energy, this essentially corresponds to the square of the field response. Furthermore, when evaluating error averages one anyway sums up the squares of the errors.

For each d_0, F may have several maxima in a search interval $\lambda_A < \lambda < \lambda_B$. When F is properly defined, each eigenvalue corresponds to a local maximum of F. It strongly depends on the number M of rough search points, whether all existing eigenvalues can be detected from the rough search data. Since the evaluation of F may be time consuming, M should be kept small. Experience with eigenvalue problems helps very much defining M and the search interval $\lambda_A < \lambda < \lambda_B$ in such a way that the computation time is reduced. When this experience is missing, one can start with rough, approximate models or other numerical evaluations such as FEM.

After the rough search, the precise location of the eigenvalues can be found rather quickly because F usually is close to a quadratic function in the neighborhood of an eigenvalue. Therefore, and iterative procedure based on parabolic approximation is fast. A very promising alternative to this is to approximate F by means of Model Based Parameter Estimation (MBPE).[22] MBPE also allows one to reduce the number M of the rough search.

Once, an eigenvalue $\lambda(d_0)$ is found, one may easily trace it for increasing or decreasing parameters d by estimating the location first from the previous results. First, when $\lambda_0 = \lambda(d_0)$ is known, one roughly estimates $\lambda_1' = \lambda_0$ and starts directly the fine search for λ_1 from here. This corresponds to a zero order extrapolation. Then one can do a linear extrapolation (using λ_0 and λ_1) to estimate the start value λ_2' for the λ_2 search, and so on. Theoretically, one can do n-th order extrapolations a soon as at least $n+1$ points are known. According to our experience, second order approximation is best. We call this Eigenvalue Estimation Technique (EET).[10] The extension of this technique to lossy, i.e., complex eigenvalue problems is straightforward. Depending on the problem, either λ or d becomes complex. MMP allows one even to assume both λ and d to be complex, but extending one of them to the complex plane increases the numerical effort already drastically. When M points are required for the rough search in the case of real λ, one often needs of order M^2 points in the complex case and therefore the computation time increases at least by the factor M, which is often of order 100. In fact, the situation is much more relaxed when one focuses on eigenvalues of practical interest because these always exhibit relatively low loss, i.e., the imaginary part is much smaller than the real part. Then, one may start with a real-valued rough search along the real axis ($\text{Im}(\lambda) = 0$) and only perform a complex fine search.

5. NUMERICAL EXAMPLE

We compute Bloch waves when the periodic structure is a rectangular array of frequency dependent dielectric cylinders in Silicon. The geometry and the material model are taken from Ref. [9]. The relative radius r of the cylinders

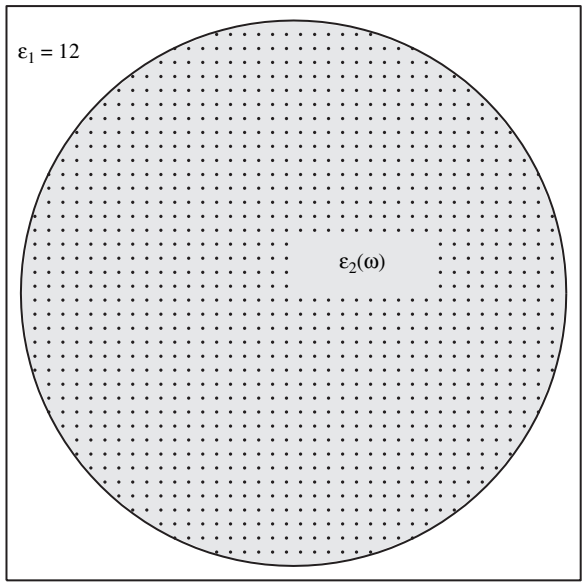

Fig. 4. Left: One cell in the periodic media. Right: The real and imaginary parts of the effective permittivity in the disc.

RESEARCH ARTICLE

with respect to the lattice constant a is 0.475. Figure 4 depicts the unit cell of the investigated photonic crystal. Silicon has the permittivity $\varepsilon_1 = 12.0$ in the chosen range of frequencies. The dielectric cylinder is a composite composed of a polymer with permittivity $\varepsilon_p = 2.56$ and quantum dots modeled by

$$\varepsilon_d(\omega) = 1 + \frac{\omega_p^2}{\omega_0^2 - \omega^2 - i\gamma\omega}$$

where $\omega_0 a/2\pi c = 0.245$ is the resonance frequency, $\omega_p = 0.8\omega_0$ is the oscillation strength, and $\gamma = 0.01\omega_0$ is the damping constant. The Maxwell-Garnett formula[23] is used to model the permittivity of the two-component composite

$$\varepsilon_2(\omega) = \varepsilon_p + \frac{3\varepsilon_p \eta\alpha(\omega)}{1 - \eta\alpha(\omega)}, \qquad \alpha(\omega) = \frac{\varepsilon_d(\omega) - \varepsilon_p}{\varepsilon_d(\omega) + 2\varepsilon_p}$$

where the quantum-dots concentration is $\eta = 0.03$ Figure 5 depict the real and imaginary parts of the frequency dependent permittivity. The composite material exhibits a frequency range with anomalous dispersion, which gives the crystal special transmittance properties.[9] We calculate the complex amplitude λ with two different finite element methods and the multiple-multipole method. The complex amplitude of the wave vector is calculated for waves propagating in the x direction. We compute the solution for 300 frequencies $\omega a/2\pi c$ in the interval $[0.176, 0.280]$.

We use FreeFEM++ with piecewise quadratic basis functions on triangular elements to discretize the problem and find a slow convergence when the size of the triangles is decreased. Therefore, very small triangles are necessary to obtain an accurate solution. The used fine

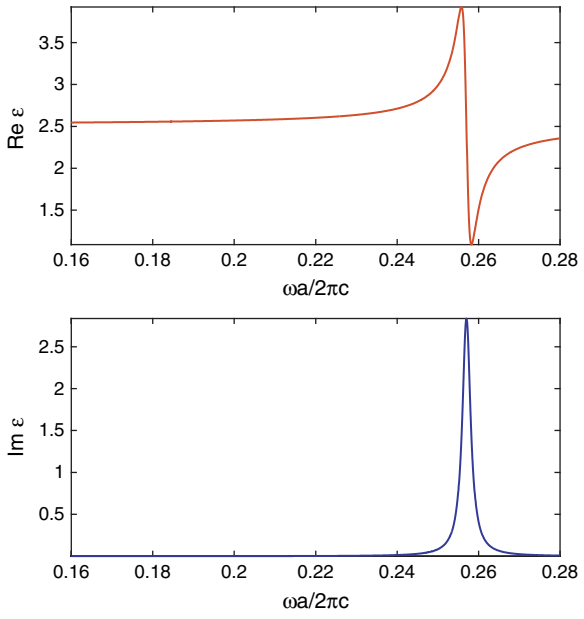

Fig. 5. Unit of the investigated photonic crystal composed of cylinders of a polymer with embedded quantum dots in Silicon.

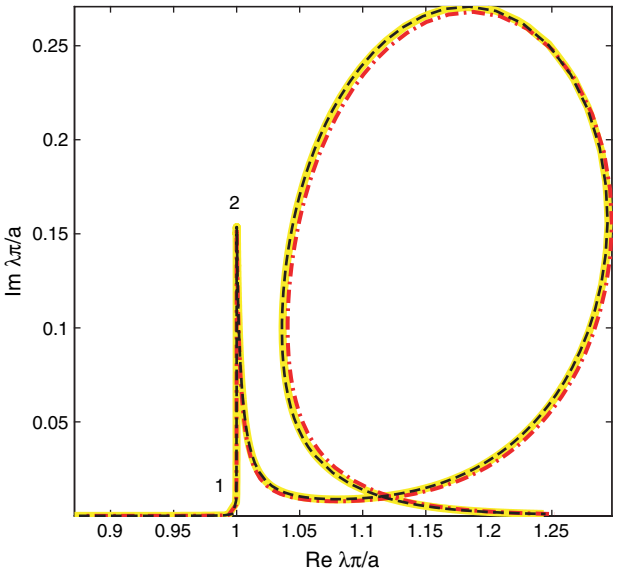

Fig. 6. The complex amplitude λ of the wave vector k is in the x-direction and the scaled frequency $\omega a/2\pi c$ is in the interval $[0.176, 0.280]$. The solid yellow line corresponds to the MMP-solution, the dashed black line corresponds to the Concepts-solution, and the dashed-dotted red line corresponds to the solution from FreeFEM++. Figures 9–12 shows the time-averaged E-field and H-Field at point 1 and point 2.

mesh leads to a quadratic eigenvalue problem with approximately 50000 unknowns at each frequency. Figure 1 depicts a coarse mesh of the type used in the calculations with FreeFEM++. The 16 eigenvalues closest to zero were computed with the finite element method and the IRA algorithm. The resulting eigenvalues are sorted and Figure 6 shows, for each frequency, the least lossy Bloch state with a positive real and imaginary part.

For the discretization with Concepts we use a mesh with 20 cells which exactly resolve the circular material interface with its edges (see Fig. 2) and different polynomial degrees. Higher polynomial degrees result in more accurate solutions. The eigenvalues are computed with the same procedure described in the last paragraph. Figure 6 shows the computed eigenvalues with polynomial degree 5 and 500 degrees of freedom. Table I show for different polynomial degrees the number of degrees of freedom and the approximated value of the eigenvalue at $\omega a/2\pi c = 0.257$.

Table I. The polynomial degree p and the number of degrees of freedom N of the p-FEM discretization. The approximated values of the eigenvalue are at the frequency $\omega a/2\pi c = 0.257$. The bold numbers show the number of correct digits when the solution with $p = 10$ is used as a reference.

p	N	Re λ	Im λ
1	20	1.33318541864574	0.19303361099020
3	180	1.24485968471827	0.25271435493168
5	500	1.24440005302382	0.25238242480122
8	1280	1.24439657853910	0.25238032743813

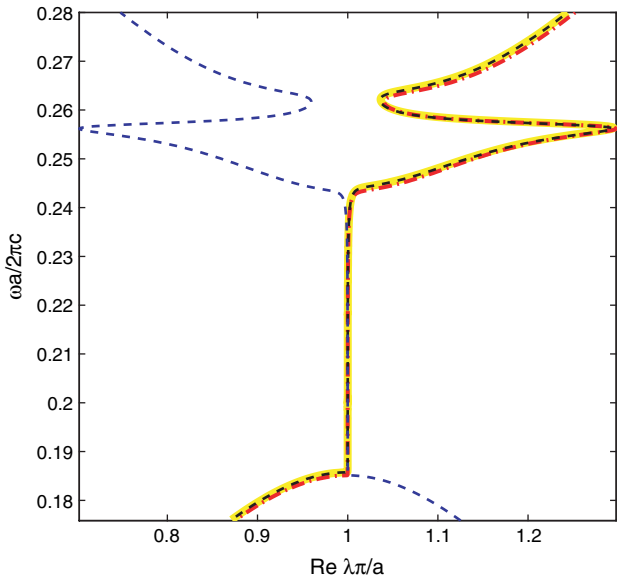

Fig. 7. The real part of the complex amplitude λ of the wave vector k is in the x-direction. The solid yellow line corresponds to the MMP-solution, the dashed black line corresponds to the Concepts-solution, and the dashed-dotted red line corresponds to the solution from FreeFEM++. The dashed blue line corresponds to (FreeFEM++) solutions with negative imaginary part of λ.

We also compute the eigenvalues with lowest loss with the MMP method. Our test case is a photonic crystal with very strong dispersion and rather large loss within a certain interval. When starting the rough search in this interval, it must be carried out in the complex plane. Therefore, it is much better to start it in an area where the loss is small. Detecting such areas is easy because this only depends

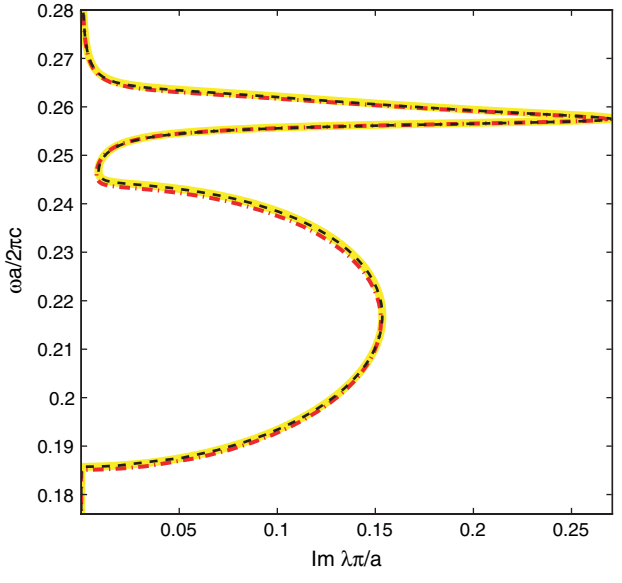

Fig. 8. The imaginary part of the complex amplitude λ of the wave vector k is in the x-direction. The solid yellow line corresponds to the MMP-solution, the dashed black line corresponds to the Concepts-solution, and the dashed-dotted red line corresponds to the solution from FreeFEM++.

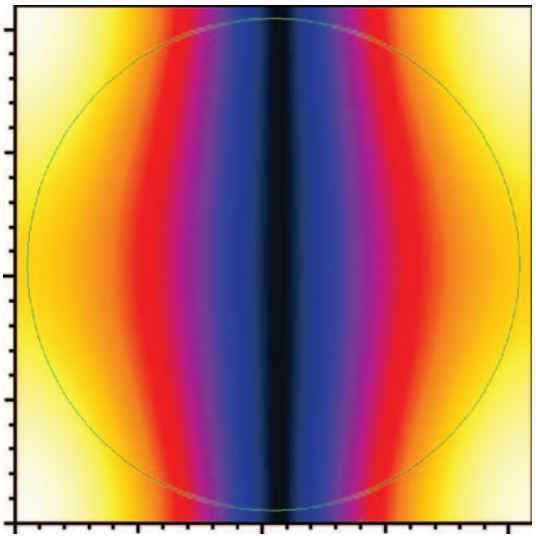

Fig. 9. The time-averaged E-field at point 1 in Figure 6. White corresponds to maximum intensity, black corresponds to 0 intensity.

on the imaginary part of the permittivity of the dispersive material. The main problem than is the following: Because of strong dispersion, the permittivity may vary rapidly within a small frequency interval (the frequency acts here as the parameter d). Thus, the EET must operate with very small frequency steps—otherwise the extrapolation may fail. As one may see from Figure 6, the trace of the complex eigenvalue exhibits a rapid change of direction of almost 90° and a sharp peak followed by a 180° change of direction. In such areas, there is a high risk that EET fails. For this reason 2000 points were used for tracing the curve shown in Figure 6, which leads to relatively long computation time. For problems with less strong dispersion it is usually sufficient to consider around 100 or even less points.

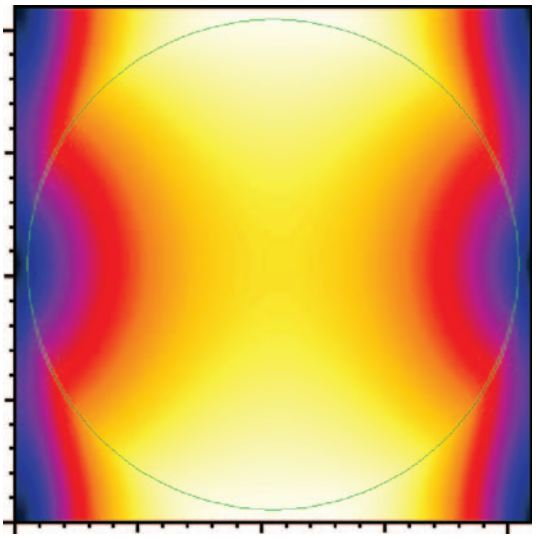

Fig. 10. The time-averaged H-field at point 1 in Figure 6. White corresponds to maximum intensity, black corresponds to 0 intensity.

RESEARCH ARTICLE

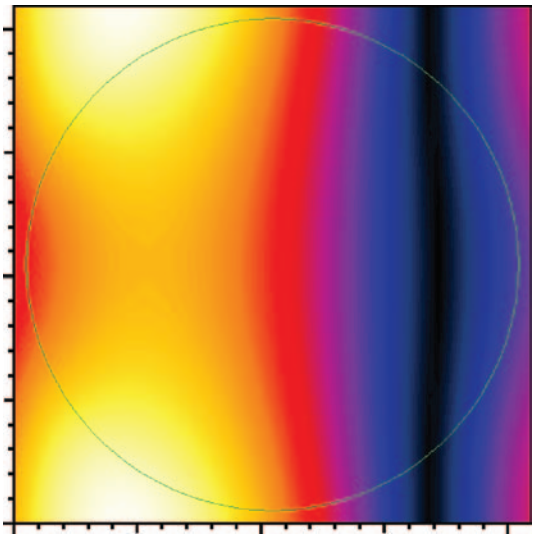

Fig. 11. The time-averaged E-field at point 2 in Figure 6. White corresponds to maximum intensity, black corresponds to 0 intensity.

Figure 6 shows that the computed eigenvalues with the MMP method and with the Concepts implementation of p-FEM are almost identical. We compare the relative l_1 error

$$l_1\text{error} = \frac{\sum_k |\lambda_{\text{method 1}}(\omega_k) - \lambda_{\text{method 2}}(\omega_k)|}{\sum_k |\lambda_{\text{method 2}}(\omega_k)|}$$

between the different finite element implementations. The summation is here over the 300 frequencies we used in the computations. The relative error between FreeFEM++ and Concepts with polynomial degree 10 is 0.01. The relative error between Concepts with polynomial degree 4 and Concepts with polynomial degree 10 is 0.0002. The computational time for the FreeFEM++ solution is about 5 hours on a standard laptop. The computational time for Concepts with polynomial degree 4 is about 1 minute.

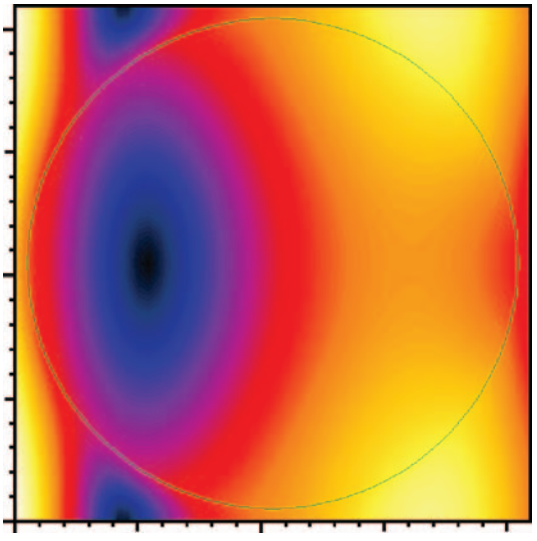

Fig. 12. The time-averaged H-field at point 2 in Figure 6. White corresponds to maximum intensity, black corresponds to 0 intensity.

The complex band structure is obtained from the real and imaginary parts of the complex wave vector k. Figures 7 and 8 show the computed complex band structure when the waves propagating in the x direction. The dashed–dotted blue line in Figure 7 corresponds to solutions with negative imaginary part of k, but we consider only solutions with a positive imaginary part. The solutions with negative imaginary part exist simultaneously with the solutions with positive imaginary part. This is clear from the symmetries of the set of Bloch waves. Figures 9–12 shows the time-averaged E-field and H-Field at the two points indicated in Figure 6. Notice that the fields change very rapidly with frequency. The electromagnetic fields were in all cases computed with the MMP method.

6. DISCUSSION AND CONCLUSIONS

We presented computations of lossy Bloch waves in dispersive and absorbing photonic crystals with the MMP method and with two different finite element methods. For given real frequencies these waves are determined from non-linear eigenvalue problems in the wave vector. The used MMP implementation (MaX-1) computes the complex amplitudes by appropriate chosen artificial sources and a search of resonances in the complex plane. With the FEM we obtained the wave vectors from a quadratic eigenvalue problem in the complex amplitude of the wave vector. We used two FEM codes for the discretization, FreeFEM++ with quadratic elements on triangles and Concepts with high order elements on curved quadrilaterals (p-FEM). The enumerated numerical methods were applied to a photonic crystal with embedded quantum dots that exhibit very strong dispersion and large loss in a frequency interval. The chosen test case is challenging as one of the material components is dispersive and lossy, and the cylindrical inclusions are close together. Nevertheless, all the used methods can compute the Bloch waves too a desired accuracy. However, the used MMP code MaX-1 and the p-FEM code Concepts distinguish themselves due to their low computational effort for very accurate solutions. This efficiency, i.e., high accuracy and small and consequently easily solvable matrix system, results from the use of higher order basis functions and an accurate description of the circular material interface. For those smooth interfaces MMP and p-FEM obtain exponential convergence.

Acknowledgments: The authors express their gratitude to Holger Brandsmeier for his implementation of part of the used functionality of Concepts. The first author acknowledges the support of the German Research Foundation (RTG 1294).

References

1. E. Yablonovitch, *Phys. Rev. Lett.* 58, 2059 **(1987)**.
2. S. John, *Phys. Rev. Lett.* 58, 2486 **(1987)**.
3. S. Johnson, Review: Fabrication Technologies for 3d Photonic Crystals, a Survey, http://ab-initio.mit.edu/photons/tutorial/L3-fab.pdf.
4. Ch. Hafner and J. Smajic, Handbook of Theoretical and Computational Nanotechnology, edited by M. Rieth and W. Schommers, American Scientific Publishers **(2006)**.
5. Ch. Hafner, J. Smajic, and D. Erni, Handbook of Theoretical and Computational Nanotechnology, edited by M. Rieth and W. Schommers, American Scientific Publishers **(2006)**.
6. K. C. Huang, E. Lidorikis, X. Jiang, J. D. Joannopoulos, K. A. Nelson, P. Bienstman, and S. Fan, *Phys. Rev. B* 69, 195111 **(2004)**.
7. M. Bergmair, K. Hingerl, and Ch. Hafner, *J. Comput. Theor. Nanosci.* 5, 717 **(2008)**.
8. M. M. Sigalas, C. M. Soukoulis, C. T. Chan, and K. M. Ho, *Phys. Rev. B* 49, 11080 **(2004)**.
9. D. Hermann, M. Diem, A. Mingaleev, A. Garcia-Martin, and K. Busch, *Phys. Rev. B* 77, 035112 **(2008)**.
10. Ch. Hafner, Post-Modern Electromagnetics: Using Intelligent MaXwell Solvers, John Wiley & Sons, Chichester **(1999)**.
11. Ch. Hafner, MaX-1: A Visual Electromagnetics Platform, John Wiley & Sons, Chichester **(1998)**.
12. C. Kittel, Introduction to Solid State Physics, John Wiley & Sons, New York **(1996)**.
13. P. Kuchment, Floquet Theory for Partial Differential Equations, Birkhauser, Basel **(1993)**.
14. C. Engström and M. Richter, On the Spectrum of an Operator Pencil with Applications to Wave Propagation in Periodic and Frequency Dependent Materials, arXiv:0803.0456v2 **(2008)**.
15. F. Tisseur and K. Meerbergen, *SIAM Rev.* 43, 235 **(2001)**.
16. R. B. Lehoucq, D. C. Sorensen, and C. Yang, ARPACK Users' Guide: Solution of Large-Scale Eigenvalue Problems with Implicitly Restarted Arnoldi Methods, SIAM Publications, Philadelphia **(1998)**.
17. Ph. Frauenfelder and Ch. Lage, *M2AN Math. Model. Numer. Anal.* 36, 937 **(2002)**.
18. C. Schwab, *p*- and *hp*- Finite Element Methods: Theory and Applications in Solid and Fluid Mechanics, Oxford University Press **(1998)**.
19. K. Schmidt and P. Kauf, *Comput. Methods Appl. Mech. Engrg.* **(2008)**, to appear.
20. A. Taflove and S. Hagness, Computational Electrodynamics: The Finite-Difference Time-Domain Method, Artech House **(2005)**.
21. E. Moreno, D. Erni, and Ch. Hafner, *Phys. Rev. B* 65, 155120 **(2002)**.
22. K. Tavzarashvili, Ch. Hafner, X. Cui, R. Vahldieck, D. Kakulia, G. Ghvedashvili, and D. Karkashadze, *J. Comput. Theor. Nanosci*, 4, 667 **(2007)**.
23. G. W. Milton, The Theory of Composites, Cambridge University Press, Cambridge, UK **(2002)**.

Received: 18 September 2008. Accepted: 29 October 2008.